Microwave imaging as applied to remote sensing making use of a multilevel fast multipole algorithm

Michael Brandfass[a] and Weng C. Chew[a]

[a]Dept. Elec. & Comp. Eng., University of Illinois, Urbana, IL 61801-2991, USA

ABSTRACT

A nonlinear reconstruction scheme based on the Distorted Born Iterative Method (DBIM) applied to metallic scatterers is presented to solve two-dimensional inverse scattering problems. By making use of half-quadratic regularization the inherently ill-posed problem of nonlinear inverse scattering can be alleviated and edges of the scatterer's profile function simultaneously be preserved. Reconstruction results are found by the minimization of a cost function.

A bistatic simulated experimental set-up is proposed in angular and frequency diversity. A Multilevel Fast Multipole Algorithm (MLFMA) in combination with a conjugate gradient (CG) scheme is introduced to solve the forward as well as the inverse scattering problem involved in the DBIM algorithm. Through the use of MLFMA for the forward and for the inverse solver, the computational complexity per CG iteration is of order $O(N \log N)$ compared to $O(N^2)$ in a standard implementation without the MLFMA.

Numerical reconstruction results obtained from synthetic scattering data are presented.

Keywords: Distorted Born Iteration Method, Multilevel Fast Multipole Algorithm, nonlinear inverse scattering, edge-preserving regularization

INTRODUCTION

Several SAR imaging schemes, which linearize the inverse scattering problem by defining a reflectivity function independent of the total field distribution on or within the scatterer are known. By this definition, linearization approximations (such as Born or Kirchhoff) are implicitly introduced and multiple interactions between scatterer and scattered field are ignored. Based on these linearizations, radar imaging of rigid scatterers such as conducting aircraft suffer from poor reconstruction results if multiple reflections occur. The Distorted Born Inversion technique accounts for nonlinear effects and does not introduce any linearization approximations. The solution is found iteratively by minimization of a cost function.[1,2] This cost function compares the measured scattered field and the computed scattered field, which is obtained by the last scatterer reconstruction update, with each other.

Angular and frequency diversity are introduced for a bistatic set-up. For the numerical implementation of the DBIM, the forward problem needs to be solved for all the excitation frequencies and incident angles of the incident fields for each scatterer update. So the bottleneck in the proposed inversion algorithm is to solve the forward problem as many times as the number of different incident angles and frequencies of the incident field to obtain the next reconstruction update. The computational complexity and the storage requirement to solve such a problem, discretized by N subscatterers via an iterative solver, (e.g. conjugate gradient method) is of order $O(N^2)$ per iteration.

To speed up the computational time, a Multilevel Fast Multipole Algorithm is introduced to solve the forward as well as the inverse problem. Storage and CPU requirements of this MLFMA solver are of order $O(N \log N)$ for each conjugate gradient iteration where N is the number of unknowns. The MLFMA recursively subdivides the reconstruction domain in a tree construction scheme and aggregates the divided subscatterers from the finest to the coarsest level. We also apply this multilevel fast multipole principle on the inverse solver by making use of an asymmetric multiple tree structure, specially adapted to DBIM for which source and observation points do not coincide with each other. Through the additional use of MLFMA for the inverse solver, the overall computational complexity remains at $O(N \log N)$.

In the first section the electromagnetic scattering problem is derived and the integral equations are discretized. In the second section the Distorted Born Inversion Scheme is introduced. The fundamentals of the MLFMA are explained

Correspondence: E-mail: michael@sunchew.ece.uiuc.edu, WWW: http://www.ifp.uiuc.edu/ lanterma/darpa;
Tel.: +1 (217) 333-4468; Fax.: +1 (217) 244-7345

in Section 3. In Section 4 the half-quadratic principles of regularization are summarized and the final iteration scheme is presented. The fifth section describes the simulated reconstruction configuration and shows the obtained reconstruction results. Thus, the objectives are:

- to implement a Multilevel Fast Multipole Algorithm for the Distorted Born Iterative Method,
- to use the MLFMA to solve the forward as well as the inverse problem in each iteration stage without storing matrices,
- to solve a two-dimensional electromagnetic inverse scattering problem for metallic scatterers.

1. FORMULATION OF THE SCATTERING PROBLEM

1.1. Derivation of the integral equations

Starting with the decoupling of Maxwell's equations for a homogeneous, isotropic medium with the permeability μ_0 and permittivity ϵ_0 equal to constant, we obtain for the total magnetic field

$$\nabla \times \left(\tilde{\epsilon}^{-1}(\mathbf{R})\nabla \times \mathbf{H}(\mathbf{R},\omega)\right) - \omega^2\mu_0\mathbf{H}(\mathbf{R},\omega) = \nabla \times \left(\tilde{\epsilon}^{-1}(\mathbf{R})\mathbf{J}_q(\mathbf{R},\omega)\right) \tag{1}$$

with

$$\tilde{\epsilon}(\mathbf{R}) = \frac{j\omega\epsilon(\mathbf{R}) - \sigma(\mathbf{R})}{j\omega} \; . \tag{2}$$

The electromagnetic scattering problem can be reduced to a scalar two-dimensional scattering problem for two different polarization cases if the scatterer is quasi two-dimensional (i.e. if the scatterer is a cylinder with infinitely long axis). We can distinguish the Transverse Magnetic (TM) case, for which the polarization vector $\hat{\mathbf{E}}_0$ of the incident field is in alignment to the cylinder axis of the scatterer, and the Transverse Electric (TE) case, for which the polarization vector is in a plane perpendicular to the scatterer's cylinder axis. In the latter case, the magnetic field $\mathbf{H}(\mathbf{R},\omega)$ has only one component in direction to this cylinder axis. Thus, we can assume for this (TE) case that $\mathbf{H}(\mathbf{R},\omega) = H_z\mathbf{e}_z$ and $H_z(x,y,z=\text{const})$. Additionally, for $\mu_0\nabla\cdot\mathbf{H}(\mathbf{R},\omega) = 0$, it follows from (1) that

$$\nabla\cdot\left(\tilde{\epsilon}^{-1}(\mathbf{R})\nabla H_z(\mathbf{R},\omega)\right) + \omega^2\mu_0 H_z(\mathbf{R},\omega) = -\nabla\times\left(\tilde{\epsilon}^{-1}(\mathbf{R})\mathbf{J}_q(\mathbf{R},\omega)\right) \; . \tag{3}$$

Inserting $\nabla\cdot\left(\epsilon_0^{-1}\nabla H_z\right)$ in Eq. (3) we can define secondary equivalent sources. With the wavenumber k for the lossless background medium $k^2 = \omega^2\mu_0\epsilon_0$ we have

$$\left[\Delta + k^2\right] H_z(\mathbf{R},\omega) = -\nabla\times\left[\mathbf{J}_q(\mathbf{R},\omega) + \mathbf{J}_c(\mathbf{R},\omega)\right]\cdot\mathbf{e}_z \tag{4}$$

$$-\nabla\times\mathbf{J}_q(\mathbf{R},\omega)\cdot\mathbf{e}_z + \nabla\cdot\left(\underbrace{\left(1-\frac{\epsilon_0}{\tilde{\epsilon}(\mathbf{R})}\right)}_{=O(\mathbf{R})}\nabla H_z(\mathbf{R},\omega)\right) \; . \tag{5}$$

The right-hand side of Eq. (4) represents the primary sources $\mathbf{J}_q(\mathbf{R},\omega)$ and the secondary equivalent sources $\mathbf{J}_c(\mathbf{R},\omega)$. The object function $O(\mathbf{R})$ is defined by the electromagnetic material parameters ϵ_0 and $\tilde{\epsilon}(\mathbf{R})$ according to Eq. (5).

Since the electromagnetic scattering problem is reduced to an equivalent scalar one, we only need to consider the free space two-dimensional scalar Green's function, given by Eq. (6):

$$G(\mathbf{R},\mathbf{R}',\omega) = \frac{j}{4}H_0^{(1)}(k|\mathbf{R}-\mathbf{R}'|) \; . \tag{6}$$

After applying the Green's theorem to Eq. (4), one obtains

$$H_z(\mathbf{R},\omega) = H_z^i(\mathbf{R},\omega) + \underbrace{\mathbf{e}_z\cdot\int_{S_M}\int\left(\nabla'\times\mathbf{J}_c(\mathbf{R}',\omega)\right)G(\mathbf{R},\mathbf{R}',\omega)\,d^2R'}_{=H_z^s(\mathbf{R},\omega)} \; . \tag{7}$$

$H_z(\mathbf{R},\omega)$, $H_z^i(\mathbf{R},\omega)$ and $H_z^s(\mathbf{R},\omega)$ in Eq. (7) are z-components of the total, the incident and the scattered magnetic field, respectively and S_M denotes the 2D-reconstruction domain which includes all the scatterers.

Partial Integration of Eq. (7) leads to a further simplification of the magnetic scattered field, according to

$$\begin{aligned} H_z^s(\mathbf{R},\omega) &= \mathbf{e}_z \cdot \int_{S_M}\int \nabla' \times [\mathbf{J}_c(\mathbf{R}',\omega)\, G(\mathbf{R},\mathbf{R}',\omega)]\, d^2R' \; - \mathbf{e}_z \cdot \int_{S_M}\int \nabla' G(\mathbf{R},\mathbf{R}',\omega) \times \mathbf{J}_c(\mathbf{R}',\omega)\, d^2R' \\ &= -\mathbf{e}_z \cdot \int_{S_M}\int \nabla' G(\mathbf{R},\mathbf{R}',\omega) \times \mathbf{J}_c(\mathbf{R}',\omega)\, d^2R' \; + \mathbf{e}_z \cdot \underbrace{\int_{C_M} \mathbf{n}' \times [\mathbf{J}_c(\mathbf{R}',\omega)\, G(\mathbf{R},\mathbf{R}',\omega)]\, dR'}_{=0} \; . \end{aligned} \tag{8}$$

The last integral of Eq. (8) is equal to zero since $\mathbf{J}_c(\mathbf{R}',\omega)$ is equal to zero on the contour C_M which describes the boundary of the reconstruction domain S_M. In the following, we want to substitute the equivalent secondary sources according to Eq. (5) in Eq. (7), for which follows:

$$H_z(\mathbf{R},\omega) = \underbrace{H_z^i(\mathbf{R},\omega) - \int_{S_M}\int \nabla' \cdot \left(\underbrace{\left(1 - \frac{\epsilon_0}{\tilde{\epsilon}(\mathbf{R}')}\right)}_{=O(\mathbf{R}')} \nabla' H_z(\mathbf{R}',\omega) \right) G(\mathbf{R},\mathbf{R}',\omega)\, d^2R'}_{=H_z^s(\mathbf{R},\omega)} \; . \tag{9}$$

By the same method used to obtain Eq. (8), it follows after performing the partial integration on Eq. (9)

$$H_z(\mathbf{R},\omega) = H_z^i(\mathbf{R},\omega) + \int_{S_M}\int O(\mathbf{R}') \nabla' H_z(\mathbf{R}',\omega) \cdot \nabla' G(\mathbf{R},\mathbf{R}',\omega)\, d^2R' \; . \tag{10}$$

1.1.1. Definitions and properties of the equivalent secondary sources

We define the object function according to Eq. (5) as

$$O(\mathbf{R}) = 1 - \frac{j\omega\epsilon_0}{j\omega\epsilon(\mathbf{R}) - \sigma(\mathbf{R})} \; . \tag{11}$$

Outside the scatterer volume S_q the conductivity $\sigma = 0$ and the permittivity ϵ is equal to the background permittivity ϵ_0. For the inner domain of the scatterer volume S_q, we suppose that $\omega\epsilon \ll \sigma$ and $\omega\epsilon_0 \ll \sigma$, which holds for all practical applications on metallic scatterers. With these assumptions, the object function becomes

$$O(\mathbf{R}) \begin{cases} \simeq 1 & \text{for} \quad \mathbf{R} \in S_c \\ 0 & \text{else} \quad \mathbf{R} \notin S_c \; . \end{cases} \tag{12}$$

In case of a perfectly electric conductor with $\sigma \longrightarrow \infty$ the object function $O(\mathbf{R})$ becomes a two-dimensional unit-step function, according to

$$\Gamma(\mathbf{R}) = \begin{cases} 1 & \text{for} \quad \mathbf{R} \in S_c \\ 0 & \text{else} \quad \mathbf{R} \notin S_c \end{cases} \tag{13}$$

which is equal to unity for $\mathbf{R}$ inside the two-dimensional scatterer domain S_c and zero outside. One can define this unit-step function by a potential function $\Phi(\mathbf{R})$ so that

$$\Gamma(\mathbf{R}) = u(\Phi(\mathbf{R})) \qquad \text{with} \qquad \Phi(\mathbf{R}) \begin{cases} < 0 & \text{for} \quad \mathbf{R} \notin V_c \cup S_c \\ = 0 & \text{for} \quad \mathbf{R} \in S_c \\ > 0 & \text{for} \quad \mathbf{R} \in V_c \setminus S_c \; . \end{cases} \tag{14}$$

Performing the derivative of this two-dimensional unit-step function as shown in Eq. (15), we can define a two-dimensional* vector singular function according to

$$\boldsymbol{\gamma}(\mathbf{R}) = -\nabla\Gamma(\mathbf{R}) = \delta(\Phi(\mathbf{R}))\, \nabla\Phi(\mathbf{R}) = \delta(\Phi(\mathbf{R}))\, |\nabla\Phi(\mathbf{R})|\, \mathbf{n} = \gamma(\mathbf{R})\, \mathbf{n} \tag{15}$$

*This is not only limited to two dimensions but can also be used for three or n dimensions.

with outward unit normal of the scatterer $\mathbf{n} = \nabla\Phi(\mathbf{R})/|\nabla\Phi(\mathbf{R})|$. With this definition we are able to find an equivalent expression to the right-hand side of Eq. (5) for the secondary equivalent current sources:

$$\mathbf{J}_c(\mathbf{R},\omega) = \gamma(\mathbf{R})\,\mathbf{J}_s(\mathbf{R},\omega) = -\mathbf{n}(\mathbf{R})\cdot\nabla\Gamma(\mathbf{R})\,\mathbf{J}_s(\mathbf{R},\omega)\ . \tag{16}$$

This secondary equivalent current density $\mathbf{J}_c(\mathbf{R},\omega)$ is singular on the contour of the scatterer and is equal to zero everywhere else according to the definitions in Eq. (15). $\mathbf{J}_s(\mathbf{R},\omega)$ is the surface current density of secondary equivalent sources and S_c is the scatterer domain enclosed by the contour C of the scatterer.

1.1.2. Integral representations for the TE-polarization

Making use of partial integrations on Eq. (10) and assuming $\sigma \longrightarrow \infty$ so that $O(\mathbf{R}) = \Gamma(\mathbf{R})$, yields

$$H_z^s(\mathbf{R},\omega) = \int\limits_C \mathbf{n}'\cdot\nabla' G(\mathbf{R},\mathbf{R}',\omega) H_z(\mathbf{R}',\omega)\,dR' - \iint\limits_{S_c} \Delta G(\mathbf{R},\mathbf{R}',\omega)\,H_z(\mathbf{R}',\omega)\,d^2R'\ . \tag{17}$$

It can be shown that the integral over S_c is equal to zero by substitution of the Green's differential equation $(\Delta + k^2)G(\mathbf{R},\mathbf{R}',\omega) = 0\ \ \forall\,\mathbf{R} \notin S_c \cup C, \mathbf{R}' \in S_c$ in Eq. (17) and subsequently making use of

$$k^2\,H_z(\mathbf{R},\omega) = \nabla\Gamma(\mathbf{R})\cdot\nabla H_z(\mathbf{R},\omega)\,,\ \ \forall\,\mathbf{R}\in S_c\ \ , \tag{18}$$

the sifting theorem for $\gamma(\mathbf{R})$ and the boundary condition for the 2D-TE-Polarization $\mathbf{n}\cdot\nabla H_z(\mathbf{R},\omega)|_{\mathbf{R}\in C} = 0$. The relation (18) can be found from (5), which is valid within the domain $\mathbf{R}\in S_c$.

By substitution of the result (17) in Eq. (7), we obtain a contour integral equation, which can be solved in discretized form for the total magnetic field from the knowledge of the normal vector $\mathbf{n} = \mathbf{n}(\mathbf{R})$:

$$H_z^i(\mathbf{R},\omega) = \int\limits_{\mathbf{R}'\in C} H_z(\mathbf{R}',\omega)\,(\delta(\mathbf{R}-\mathbf{R}') - \mathbf{n}(\mathbf{R}')\cdot\nabla' G(\mathbf{R},\mathbf{R}',\omega))\,dR'\ . \tag{19}$$

From the knowledge of the total magnetic field $H_z(\mathbf{R},\omega)$ in the reconstruction domain we can determine the scattered magnetic field on the measurement surface. For the total magnetic field in the reconstruction domain, it follows that

$$H_z(\mathbf{R},\omega) = H_z^i(\mathbf{R},\omega) + \underbrace{\int\limits_{\mathbf{R}'\in C} H_z(\mathbf{R}',\omega)\,\mathbf{n}(\mathbf{R}')\cdot\nabla' G(\mathbf{R},\mathbf{R}',\omega)\,dR'}_{=\,H_z^s(\mathbf{R},\omega)} \tag{20}$$

where $\mathbf{R}$ is the observation point vector. Analogously, for the scattered magnetic field on the measurement surface $H_z^{sM}(\mathbf{R},\omega)$ we have

$$H_z^{sM}(\mathbf{R},\omega) = \int\limits_{\mathbf{R}'\in C} H_z(\mathbf{R}',\omega)\,\mathbf{n}(\mathbf{R}')\cdot\nabla' G(\mathbf{R},\mathbf{R}',\omega)\,dR' \tag{21}$$

with $\mathbf{R}$ as the observation point vector pointing to the measurement surface.

1.1.3. Integral representations for the TM-polarization

In a similar way we can find the analogous formulas to Eq. (19) and (21) for the TM-polarization considering perfectly electric conducting scatterers. We want to have access to the components of the normal field $\mathbf{n}(\mathbf{R})$ of the scatterer rather than the current $\mathbf{J}_s(\mathbf{R})$ on the scatterer. Additionally, the derived reconstruction procedure for the TM-polarization should be formally equivalent to the TE-case. To comply with these requirements, we have to perform a gradient operation on the TM-polarization formulas, yielding

$$\nabla E_z^i(\mathbf{R},\omega) = \int\limits_{\mathbf{R}'\in C} \nabla' E_z(\mathbf{R}',\omega)\cdot\left(\mathbf{I}\delta(\mathbf{R}-\mathbf{R}') - \mathbf{n}(\mathbf{R}')\right)\nabla' G(\mathbf{R},\mathbf{R}',\omega)dR' \tag{22}$$

and

$$\nabla E_z^{sM}(\mathbf{R},\omega) = \int\limits_{\mathbf{R}'\in C} \mathbf{n}(\mathbf{R}')\cdot\nabla' E_z(\mathbf{R}',\omega)\,\nabla' G(\mathbf{R},\mathbf{R}',\omega)\,dR' \tag{23}$$

1.2. Discretation of the field integral equations

The Method of the Moments is used to discretize the pertinent integral equations via pulse-basis functions and point matching for testing.

The numerical implementation of the integration over the discretized contour elements C_w is performed by Gauss-Legendre quadrature rule and the length of the integration elements C_w are chosen by the diameters of equivalent sized circles of the discretation patches in the reconstruction domain.

1.3. Introduction of the vector and matrix notation

Equation (19) and Eq. (22) can be written in matrix notation with the Green's matrix $\overline{\mathbf{G}}_{CC}$ which consists of the vector-elements of the free space Green's function. These vector-elements can be split into two components – one for the x and the other for the y-direction so that the matrix $\overline{\mathbf{G}}_{CC}$ consists of two submatrices with L as the number of sources and observation point elements on the scatterer surface. Thus, for the total electric field on the surface of the scatterer follows

$$\mathbf{E}_C^{\nabla;[2L\times 1]}(\omega) = \left(\overline{\mathbf{I}}^{[2L\times 2L]} - \overline{\mathbf{G}}_{CC}^{[2L\times L]}(\omega)\cdot\overline{\mathbf{n}}^{[L\times 2L]}\right)^{-1}\cdot\mathbf{E}_{C;i}^{\nabla;[2L\times 1]}(\omega) \qquad \text{with} \tag{24}$$

$$\mathbf{E}_{C;i}^{\nabla;[2L\times 1]} = \left[\partial_x E_z^i(\mathbf{R}_1),\ldots,\partial_x E_z^i(\mathbf{R}_L)\mid\partial_y E_z^i(\mathbf{R}_1),\ldots,\partial_y E_z^i(\mathbf{R}_L)\right]^T \tag{25}$$

$$\mathbf{E}_C^{\nabla;[2L\times 1]} = \left[\partial_x E_z(\mathbf{R}_1),\ldots,\partial_x E_z(\mathbf{R}_L)\mid\partial_y E_z(\mathbf{R}_1),\ldots,\partial_y E_z(\mathbf{R}_L)\right]^T \tag{26}$$

$$\overline{\mathbf{n}}^{[L\times 2L]} = \left[\begin{array}{ccc|ccc} n_1^x(\mathbf{R}_1) & \ldots & 0 & n_1^y(\mathbf{R}_1) & \ldots & 0 \\ \vdots & \ddots & \vdots & \vdots & \ddots & \vdots \\ 0 & \ldots & n_L^x(\mathbf{R}_L) & 0 & \ldots & n_L^y(\mathbf{R}_L)\end{array}\right];\quad \overline{\mathbf{G}}_{CC}^{[2L\times L]} = \left[\begin{array}{ccc} g_1^x(\mathbf{R}_1) & \ldots & g_1^x(\mathbf{R}_L) \\ \vdots & \ddots & \vdots \\ g_L^x(\mathbf{R}_1) & \ldots & g_L^x(\mathbf{R}_L) \\ \hline g_1^y(\mathbf{R}_1) & \ldots & g_1^y(\mathbf{R}_L) \\ \vdots & \ddots & \vdots \\ g_L^y(\mathbf{R}_1) & \ldots & g_L^y(\mathbf{R}_L)\end{array}\right] \tag{27}$$

For the total magnetic field, it follows that:

$$\mathbf{H}_C^{[L\times 1]}(\omega) = \left(\overline{\mathbf{I}}^{[L\times L]} - \overline{\mathbf{G}}_{CC}^{[L\times 2L]}(\omega)\cdot\overline{\mathbf{n}}^{[2L\times L]}\right)^{-1}\cdot\mathbf{H}_{C;i}^{[L\times 1]}(\omega) \qquad \text{where we have} \tag{28}$$

$$\mathbf{H}_{C;i}^{[L\times 1]} = \left[H_z^i(\mathbf{R}_1),H_z^i(\mathbf{R}_2),\ldots,H_z^i(\mathbf{R}_v),\ldots,H_z^i(\mathbf{R}_L)\right]^T \tag{29}$$

$$\mathbf{H}_C^{[L\times 1]} = \left[H_z(\mathbf{R}_1),H_z(\mathbf{R}_2),\ldots,H_z(\mathbf{R}_w),\ldots,H_z(\mathbf{R}_L)\right]^T \tag{30}$$

$$\overline{\mathbf{G}}_{CC}^{[L\times 2L]} = \left[\begin{array}{ccc|ccc} g_1^x(\mathbf{R}_1) & \ldots & g_1^x(\mathbf{R}_L) & g_1^y(\mathbf{R}_1) & \ldots & g_1^y(\mathbf{R}_L) \\ \vdots & \ddots & \vdots & \vdots & \ddots & \vdots \\ g_L^x(\mathbf{R}_1) & \ldots & g_L^x(\mathbf{R}_L) & g_L^y(\mathbf{R}_1) & \ldots & g_L^y(\mathbf{R}_L)\end{array}\right];\quad \overline{\mathbf{n}}^{[2L\times L]} = \left[\begin{array}{ccc} n_1^x(\mathbf{R}_1) & \ldots & 0 \\ \vdots & \ddots & \vdots \\ 0 & \ldots & n_L^x(\mathbf{R}_L) \\ \hline n_1^y(\mathbf{R}_1) & \ldots & 0 \\ \vdots & \ddots & \vdots \\ 0 & \ldots & n_L^y(\mathbf{R}_L)\end{array}\right]. \tag{31}$$

$\overline{\mathbf{n}}$ is a matrix which consists of two submatrices which contain the scatterer surface normal components n_x and n_y. Both these submatrices are diagonal.

In the same manner we obtain the electric and magnetic scattered field on the measurement surface according to

$$\mathbf{E}_{Calc;s}^{\nabla;[2M\times 1]}(\omega) = \overline{\mathbf{G}}_{MC}^{[2M\times L]}(\omega)\cdot\overline{\mathbf{n}}^{[L\times 2L]}\cdot\mathbf{E}_C^{\nabla;[2L\times 1]}(\omega) \tag{32}$$

and

$$\mathbf{H}_{Calc;s}^{[M\times 1]}(\omega) = \overline{\mathbf{G}}_{MC}^{[M\times 2L]}(\omega)\cdot\overline{\mathbf{n}}^{[2L\times L]}\cdot\mathbf{H}_C^{[L\times 1]}(\omega) \tag{33}$$

where $\mathbf{E}_{Calc;s}^{\nabla;[2M\times 1]}$, $\mathbf{H}_{Calc;s}^{[M\times 1]}$ are the computed differential scattered electric field and the computed magnetic field on the measurement surface, respectively. $\mathbf{E}_{C}^{\nabla;[2L\times 1]}$, $\mathbf{H}_{C}^{[L\times 1]}$ are the differential total electric and the total magnetic field on the scatterer contour. $\overline{\mathbf{G}}_{MC}$ is the Green's matrix which connects the contour of the scatterer with the measurement surface. The L-index denotes the total number of samples for the contour of the scatterer and the M-index denotes the number of samples on the measurement surface.

2. FORMULATION OF THE INVERSE PROBLEM

2.1. Distorted Born Iterative Method

The discretized matrix equation of the scattered field (33) depends, apart from the frequency ω, on the discretized scatterer elements in form of the diagonal matrix $\overline{\mathbf{n}}$. Thus, we can derive the *Frechet*-derivative of Eq. (33) with respect to all the elements of $\overline{\mathbf{n}}$ to obtain a Newton-type minimization scheme to find a scatterer update, iteratively. It follows from Eq. (33) for the TE-polarization

$$\delta\mathbf{H}_{s}^{[M\times 1]} = \overline{\mathbf{G}}_{MC}^{[M\times 2L]} \cdot \left(\overline{\mathbf{n}}^{[2L\times L]} \cdot \delta\mathbf{H}_{C}^{[L\times 1]} + \overline{\mathbf{H}}_{C}^{[2L\times 2L]} \cdot \delta\mathbf{n}^{[2L\times 1]} \right) . \tag{34}$$

In Eq. (34) we still need to derive the discretized total magnetic field $\mathbf{H}_{C}^{[L\times 1]}$ in the reconstruction domain with respect to $\mathbf{n}^{[2L\times 1]}$. Hence, we have

$$\delta\mathbf{H}_{C}^{[L\times 1]} = \delta\left(\left(\overline{\mathbf{I}}^{[L\times L]} - \overline{\mathbf{G}}_{CC}^{[L\times 2L]} \cdot \overline{\mathbf{n}}^{[2L\times L]} \right)^{-1} \right) \cdot \mathbf{H}_{C;i}^{[L\times 1]} . \tag{35}$$

It can further be shown that

$$\delta\overline{\mathbf{A}}^{-1} = -\overline{\mathbf{A}}^{-1} \cdot \delta\overline{\mathbf{A}} \cdot \overline{\mathbf{A}}^{-1} \tag{36}$$

holds as long as $\overline{\mathbf{A}}$ is regular. Substituting Eq. (36) in Eq. (35) with $\overline{\mathbf{A}} = (\overline{\mathbf{I}} - \overline{\mathbf{G}}_{CC} \cdot \overline{\mathbf{n}})$ and the result of this in Eq. (34), yields

$$\delta\mathbf{H}_{s}^{[M\times 1]} = \overline{\mathbf{G}}_{MC}^{[M\times 2L]} \cdot \left[\overline{\mathbf{I}}^{[2L\times 2L]} + \overline{\mathbf{n}}^{[2L\times L]} \cdot \left(\overline{\mathbf{I}}^{[L\times L]} - \overline{\mathbf{G}}_{CC}^{[L\times 2L]} \cdot \overline{\mathbf{n}}^{[2L\times L]} \right)^{-1} \cdot \overline{\mathbf{G}}_{CC}^{[L\times 2L]} \right] \cdot \overline{\mathbf{H}}_{C}^{[2L\times 2L]} \cdot \delta\mathbf{n}^{[2L\times 1]} \tag{37}$$

with

$$\delta\mathbf{H}_{s}^{[M\times 1]} = \mathbf{H}_{Meas;s}^{[M\times 1]} - \mathbf{H}_{Calc;s}^{[M\times 1]} \qquad \text{and} \qquad \mathbf{n}_{\nu+1}^{[2L\times 1]} = \mathbf{n}_{\nu}^{[2L\times 1]} + \delta\mathbf{n}_{\nu}^{[2L\times 1]} . \tag{38}$$

ν is the iteration number of the current scatterer update.

Equation (37) can be simplified by making use of the series expansion of the matrix $(\overline{\mathbf{I}} - \overline{\mathbf{G}}_{CC} \cdot \overline{\mathbf{n}})^{-1}$ so that it finally follows that

$$\begin{aligned} \delta\mathbf{H}_{s} = \; & = \overline{\mathbf{G}}_{MC} \cdot \left[\overline{\mathbf{I}} + \overline{\mathbf{n}} \cdot \left(\overline{\mathbf{I}} - \overline{\mathbf{G}}_{CC} \cdot \overline{\mathbf{n}} \right)^{-1} \cdot \overline{\mathbf{G}}_{CC} \right] \cdot \overline{\mathbf{H}}_{C} \cdot \delta\mathbf{n} \\ & = \overline{\mathbf{G}}_{MC} \cdot \left(\overline{\mathbf{I}} - \overline{\mathbf{n}} \cdot \overline{\mathbf{G}}_{CC} \right)^{-1} \cdot \delta\overline{\mathbf{n}} \cdot \left(\overline{\mathbf{I}} - \overline{\mathbf{G}}_{CC} \cdot \overline{\mathbf{n}} \right)^{-1} \cdot \mathbf{H}_{C;i} \end{aligned} \tag{39}$$

with

$$\overline{\mathbf{G}}_{MC}^{[M\times 2L]} = \left[\overline{\mathbf{G}}_{MC}^{x} \;\middle|\; \overline{\mathbf{G}}_{MC}^{y} \right] ; \quad \overline{\mathbf{G}}_{CC}^{[L\times 2L]} = \left[\overline{\mathbf{G}}_{CC}^{x} \;\middle|\; \overline{\mathbf{G}}_{CC}^{y} \right] ; \quad \overline{\mathbf{H}}_{C}^{[2L\times 2L]} = \left[\begin{array}{c|c} \overline{\mathbf{H}} & \overline{\mathbf{0}} \\ \hline \overline{\mathbf{0}} & \overline{\mathbf{H}} \end{array} \right] \tag{40}$$

$$\overline{\mathbf{n}}^{[2L\times L]} = \left[\begin{array}{c} \overline{\mathbf{n}}_{x} \\ \hline \overline{\mathbf{n}}_{y} \end{array} \right] , \qquad \delta\mathbf{n}^{[2L\times 1]} = \left[\begin{array}{c} \mathbf{n}_{x} \\ \hline \mathbf{n}_{y} \end{array} \right] . \tag{41}$$

The submatrices $\overline{\mathbf{H}}$ in $\overline{\mathbf{H}}_{C}^{[2L\times 2L]}$ are diagonal and identical. The matrices which need to be inverted in Eq. (39) can now be written as

$$\left(\overline{\mathbf{I}} - \overline{\mathbf{G}}_{CC} \cdot \overline{\mathbf{n}} \right) = \left[\overline{\mathbf{I}} - \left(\overline{\mathbf{G}}_{CC}^{x} \cdot \overline{\mathbf{n}}_{x} + \overline{\mathbf{G}}_{CC}^{y} \cdot \overline{\mathbf{n}}_{y} \right) \right]^{[L\times L]} , \tag{42}$$

$$\left(\overline{\mathbf{I}} - \overline{\mathbf{n}} \cdot \overline{\mathbf{G}}_{CC} \right) = \left[\begin{array}{c|c} \overline{\mathbf{I}} - \overline{\mathbf{n}}_{x} \cdot \overline{\mathbf{G}}_{CC}^{x} & \overline{\mathbf{n}}_{x} \cdot \overline{\mathbf{G}}_{CC}^{y} \\ \hline \overline{\mathbf{n}}_{y} \cdot \overline{\mathbf{G}}_{CC}^{x} & \overline{\mathbf{I}} - \overline{\mathbf{n}}_{y} \cdot \overline{\mathbf{G}}_{CC}^{y} \end{array} \right]^{[2L\times 2L]} . \tag{43}$$

For the TM-polarization we can derive an equivalent formula to Eq. (39) in the same way. It follows that:

$$\begin{aligned}\delta\mathbf{E}_s^{\nabla} &= \overline{\mathbf{G}}_{MC}\cdot\left[\overline{\mathbf{I}}+\overline{\mathbf{n}}\cdot\left(\overline{\mathbf{I}}-\overline{\mathbf{G}}_{CC}\cdot\overline{\mathbf{n}}\right)^{-1}\cdot\overline{\mathbf{G}}_{CC}\right]\cdot\ \overline{\mathbf{E}}_C^{\nabla}\cdot\delta\mathbf{n}\\ &= \overline{\mathbf{G}}_{MC}\cdot\left(\overline{\mathbf{I}}-\overline{\mathbf{n}}\cdot\overline{\mathbf{G}}_{CC}\right)^{-1}\cdot\delta\overline{\mathbf{n}}\cdot\left(\overline{\mathbf{I}}-\overline{\mathbf{G}}_{CC}\cdot\overline{\mathbf{n}}\right)^{-1}\cdot\mathbf{E}_{C;i}^{\nabla}\end{aligned} \tag{44}$$

with

$$\overline{\mathbf{n}}^{[L\times 2L]}=\left[\overline{\mathbf{n}}_x\ \middle|\ \overline{\mathbf{n}}_y\right];\quad \delta\overline{\mathbf{n}}^{[2L\times 1]}=\begin{bmatrix}\delta\mathbf{n}_x\\ \delta\mathbf{n}_y\end{bmatrix};\quad \overline{\mathbf{E}}_C^{\nabla;[L\times 2L]}=\left[\ \overline{\mathbf{E}}_x^{\partial_x}\ \middle|\ \overline{\mathbf{E}}_y^{\partial_y}\ \right] \tag{45}$$

$$\overline{\mathbf{G}}_{MC}^{[2M\times L]}=\begin{bmatrix}\overline{\mathbf{G}}_{MC}^{x}\\ \overline{\mathbf{G}}_{MC}^{y}\end{bmatrix},\qquad \overline{\mathbf{G}}_{CC}^{[2L\times L]}=\begin{bmatrix}\overline{\mathbf{G}}_{CC}^{x}\\ \overline{\mathbf{G}}_{CC}^{y}\end{bmatrix}. \tag{46}$$

where

$$\left(\overline{\mathbf{I}}-\overline{\mathbf{n}}\cdot\overline{\mathbf{G}}_{CC}\right)=\left[\overline{\mathbf{I}}-\left(\overline{\mathbf{G}}_{CC}^{x}\cdot\overline{\mathbf{n}}_x+\overline{\mathbf{G}}_{CC}^{y}\cdot\overline{\mathbf{n}}_y\right)\right]^{[L\times L]}, \tag{47}$$

$$\left(\overline{\mathbf{I}}-\overline{\mathbf{G}}_{CC}\cdot\overline{\mathbf{n}}\right)=\begin{bmatrix}\overline{\mathbf{I}}-\overline{\mathbf{n}}_x\cdot\overline{\mathbf{G}}_{CC}^{x} & \mid & \overline{\mathbf{n}}_y\cdot\overline{\mathbf{G}}_{CC}^{x}\\ \overline{\mathbf{n}}_x\cdot\overline{\mathbf{G}}_{CC}^{y} & \mid & \overline{\mathbf{I}}-\overline{\mathbf{n}}_y\cdot\overline{\mathbf{G}}_{CC}^{y}\end{bmatrix}^{[2L\times 2L]}. \tag{48}$$

To select elements for the scatterer contour from the elements of the previous iteration contained in the matrix $\overline{\mathbf{n}}$, we have to introduce a threshold above which all the selected elements are treated as elements of the scatterer. With this threshold, we can fill up a new vector $\mathbf{H}_C^{[L\times 1]}$ or $\mathbf{E}_{C;i}^{\nabla;[2L\times 1]}$ from the computed magnetic or electric field of the previous iteration, respectively. With this procedure, the size of the investigated reconstruction problem shrinks with the subsequent iteration process and approaches closer to the contour of the original scattering object to be reconstructed without any *a priori* knowledge.

We used a conjugate gradient (CG) scheme to invert the matrix equation (28) of the forward problem as well as to invert Eq. (37) of the inverse problem. For solving the matrix equation (28) the product $\overline{\mathbf{G}}_{CC}\cdot\mathbf{J}_s$ needs to be computed i times where i is the number of CG iterations and $\mathbf{J}_s=\overline{\mathbf{n}}\cdot\mathbf{H}_C$. Instead of computing the matrix-vector product directly which has a computational complexity of $\mathcal{O}(L^2)$, a Multilevel Fast Multipole Algorithm (MLFMA) was used which has a computational complexity of $\mathcal{O}(L\log(L))$.

3. FUNDAMENTALS OF THE MULTILEVEL FAST MULTIPOLE ALGORITHM

The principle of the MLFMA is that the interactions of source and observation points, which are represented by the Green's matrices $\overline{\mathbf{G}}_{CC}$ and $\overline{\mathbf{G}}_{MC}$ are split up by aggregation of source points and disaggregation of observation points to source point groups and observation point groups, respectively. Only the source point and observation point group representatives interact with each other and each source and each observation point only interact with its related source point group and observation point group representative. With this principle the number of total interactions can be reduced from $N\times M$ source-observation-point interactions, where N is the number of source and M the number of observation points, to $N+\frac{N}{L_s}\cdot\frac{M}{L_{ob}}+M$ number of interactions with L_s and L_{ob} as the number of source and observation point groups, respectively. Figure 1 illustrates the reduction of interactions by aggregating source and disaggregating observation points to groups. To aggregate source and disaggregate observation points we have to introduce the aggregated source-point and disaggregated observation-point locations in the argument of the first order and first kind Hankel function which represents the elements of the Green's matrices $\overline{\mathbf{G}}_{CC}$ and $\overline{\mathbf{G}}_{MC}$. With

$$H_\nu^{(1)}(k|\mathbf{R}_j-\mathbf{R}_i|)\,\mathrm{e}^{j\nu\varphi_{ji}}=H_\nu^{(1)}(kr_{ji})\,\mathrm{e}^{j\nu\varphi_{ji}} \tag{49}$$

we can define aggregated source-point and disaggregated observation-point locations grouping source-points and observation points, according to

$$\mathbf{r}_{ji}=\underbrace{\mathbf{R}_j-\mathbf{R}_{l'}}_{=\mathbf{r}_{jl'}}+\underbrace{\mathbf{R}_{l'}-\mathbf{R}_l}_{=\mathbf{r}_{l'l}}+\underbrace{\mathbf{R}_l-\mathbf{R}_i}_{=\mathbf{r}_{li}} \tag{50}$$

where $\mathbf{R}_i$ and $\mathbf{R}_j$ are the source-point and the observation-point locations, respectively. $\mathbf{R}_l$ and $\mathbf{R}_{l'}$ are the aggregated source-point and the disaggregated observation-point locations.

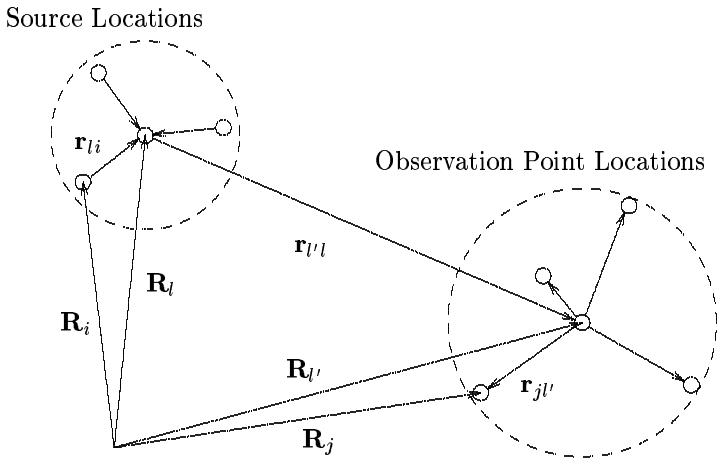

Figure 1. FMM – Interactions

After a two-stage application of the Hankel function addition theorem with $|\mathbf{r}_{li}| < |\mathbf{r}_{l'l}|$ and $|\mathbf{r}_{jl'}| < |\mathbf{r}_{l'i}|$, it follows from Eq. (49)

$$H_\nu^{(1)}(kr_{ji})\,\mathrm{e}^{j\nu\varphi_{ji}} = \mathrm{e}^{j\nu(\varphi_{l'l}+\pi)} \sum_m J_m(kr_{jl'})\,\mathrm{e}^{jm(\varphi_{jl'}-\pi)} \sum_n H_{m-n-\nu}^{(1)}(kr_{l'l})\,\mathrm{e}^{-j(m-n)\varphi_{l'l}} J_n(kr_{li})\,\mathrm{e}^{-jn\varphi_{li}} \,. \tag{51}$$

Now, we can introduce the integral representation of the Bessel functions according to

$$J_m(kr_{jl'})\,\mathrm{e}^{\pm jm\varphi_{jl'}} = \frac{1}{2\pi} \int_{-\pi}^{\pi} \mathrm{e}^{jkr_{jl'}\cos(\vartheta\mp\varphi_{jl'})}\,\mathrm{e}^{jm(\vartheta-\pi/2)}\,d\vartheta \tag{52}$$

and exchange the order of the integrals with the series expansion. After making use of the sifting property of the δ-distribution, we obtain

$$H_\nu^{(1)}(kr_{ji})\,\mathrm{e}^{j\nu\varphi_{ji}} = \frac{\mathrm{e}^{j\nu\pi}}{2\pi} \int_{-\pi}^{\pi} \beta_{jl'}(\vartheta)\alpha_{l'l}(\vartheta)\beta_{li}(\vartheta)\,d\vartheta \tag{53}$$

with

$$\beta_{jl'}(\vartheta) = \mathrm{e}^{jkr_{jl'}\cos(\vartheta-\varphi_{jl'})}\,; \qquad \alpha_{l'l}(\vartheta) = \sum_p j^p\,\mathrm{e}^{j\vartheta p}\,H_{p-\nu}^{(1)}(kr_{l'l})\,\mathrm{e}^{-j(p-\nu)\varphi_{l'l}}\,; \qquad \beta_{li}(\vartheta) = \mathrm{e}^{jkr_{li}\cos(\vartheta-\varphi_{li})} \tag{54}$$

for which the integration over ϑ can be expressed by a Q-point summation

$$H_\nu^{(1)}(kr_{ji})\,\mathrm{e}^{j\nu\varphi_{ji}} = \frac{\mathrm{e}^{j\nu\pi}}{Q} \sum_{q=1}^{Q} \beta_{jl'}(\vartheta_q)\alpha_{l'l}(\vartheta_q)\beta_{li}(\vartheta_q) \tag{55}$$

with the aggregation operator $\underline{\beta}_{jl'}$, the disaggregation operator $\underline{\beta}_{li}$ and the diagonalized translation operator $\overline{\alpha}_{l'l}$ in accordance with:

$$\underline{\beta}_{jl'} = \begin{pmatrix} \beta_{jl'}(\vartheta_1) \\ \vdots \\ \beta_{jl'}(\vartheta_Q) \end{pmatrix}\,; \quad \underline{\beta}_{li} = \begin{pmatrix} \beta_{li}(\vartheta_1) \\ \vdots \\ \beta_{li}(\vartheta_Q) \end{pmatrix}\,; \quad \overline{\alpha}_{l'l} = \begin{pmatrix} \alpha_{l'l}(\vartheta_1) & \dots & 0 \\ \vdots & \ddots & \vdots \\ 0 & \dots & \alpha_{l'l}(\vartheta_Q) \end{pmatrix}\,. \tag{56}$$

Now, we are able to nest this algorithm into itself by the aggregation of the source point groups and the disaggregation of the observation point groups to bigger source and observation point groups, respectively. For $\mathcal{O}(N)$ number of source and observation points, this Fast Multipole Algorithm can be $\log(N)$ times nested into itself which leads to the tree structure of the MLFMA in Figure 2. Basically, in MLFMA cylindrical waves are replaced by an integration (summation) of plane waves which lead to the diagonalization of the translation operator α. Each level has a computational complexity of $\mathcal{O}(N)$. Thus, with $\log(N)$-levels the total cost is $\mathcal{O}(N\log(N))$.[3,4] Apart from the lower computational complexity, the storage requirement using MLFMA is also only $\mathcal{O}(N\log(N))$ compared to direct computation requiring $\mathcal{O}(N^2)$ memory.

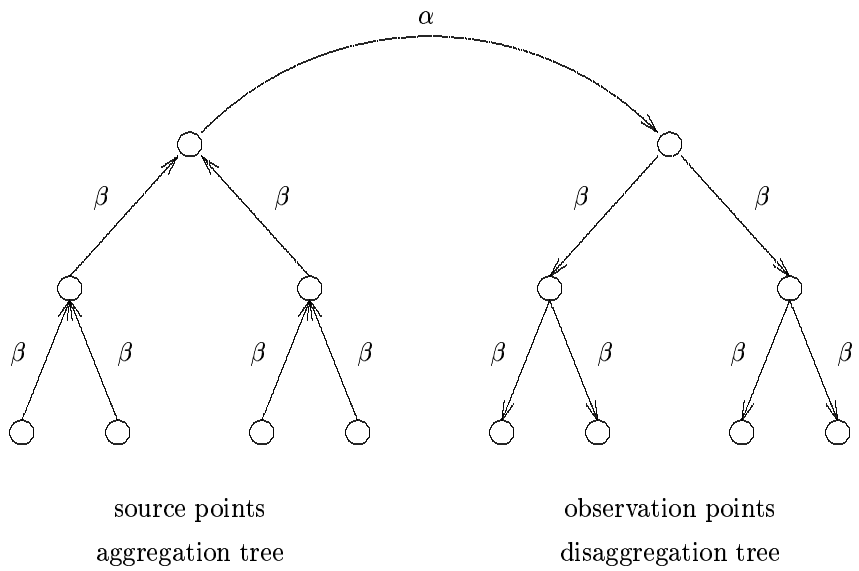

Figure 2. MLFMA – Tree Structure

4. HALF-QUADRATIC REGULARIZATION

Usually, the number of samples M on the measurement surface is less than the number of cells N in the reconstruction domain resulting in an under-determined matrix equation Eq. (39). By just increasing the number of observation-points on the measurement surface, so that M becomes equal to N, one does not solve the problem, since the added measurement data resemble each other due to a denser sampling on the measurement surface, which leads to a very ill-conditioned matrix equation. But since the matrix equation (39) also depends on the frequency ω and the angle of the incident field, we can consider frequency and/or angular diversity to build a matrix equation system with most possibly diverse scattering data information. Additionally, a regularization scheme needs to be introduced to overcome the still ill-conditioned matrix equation system. We choose the principle of half-quadratic regularization which has the property of preserving edges while homogeneous domains of the object function are smoothed.[5,6]

From Eq. (39), we can build a matrix equation system which includes all the different frequency and/or angular diversity experiments. The normal equation of such an unconstrained minimization problem is

$$\left(\overline{\mathbf{A}}^T \cdot \overline{\mathbf{A}} + \lambda \overline{\mathbf{D}}^T \cdot \overline{\mathbf{B}}^T \cdot \overline{\mathbf{B}} \cdot \overline{\mathbf{D}}\right) \cdot \delta\mathbf{n} = \overline{\mathbf{A}}^T \cdot \mathbf{d} \tag{57}$$

where $\delta\mathbf{n}$ is the object function update. The object function for perfect electric conducting scatterers is a real quantity. The $\mathbf{d}$-vector contains the differences between the computed scattered field from the last reconstruction update and the measured scattered field in accordance with Eq. (38) but for all the different frequency and/or angular diversity experiments. The matrix $\overline{\mathbf{B}}$ in Eq. (57) consists of eight diagonal submatrices, according to

$$\overline{\mathbf{B}} = [\mathrm{diag}\{\sqrt{(b_x^x)_l}\}, \mathrm{diag}\{\sqrt{(b_y^x)_l}\}, \mathrm{diag}\{\sqrt{(b_y^x)_l}\}, \ldots, \mathrm{diag}\{\sqrt{(b_{d1}^y)_l}\}, \mathrm{diag}\{\sqrt{(b_{d2}^x)_l}\}, \mathrm{diag}\{\sqrt{(b_{d2}^y)_l}\}]^T \,. \tag{58}$$

These diagonal submatrices contain the regularization weights for the numerically computed gradients corresponding to the differences of the elements in the x, y, and both diagonal-directions. Since $\delta\mathbf{n}$ contains the update of the normal elements of both Cartesian directions, the total number of submatrices contained in $\overline{\mathbf{B}}$ has to be eight. $\overline{\mathbf{D}}$ is the matrix which also consists of eight submatrices to perform the gradient computation for the pertinent directions, according to

$$\overline{\mathbf{D}} = [\{\overline{\mathbf{D}}_x^x\}^T, \{\overline{\mathbf{D}}_x^y\}^T, \{\overline{\mathbf{D}}_y^x\}^T, \{\overline{\mathbf{D}}_y^y\}^T, \{\overline{\mathbf{D}}_{d1}^x\}^T, \{\overline{\mathbf{D}}_{d1}^x\}^T, \{\overline{\mathbf{D}}_{d2}^x\}^T, \{\overline{\mathbf{D}}_{d2}^x\}^T]^T \tag{59}$$

where for instance the submatrix $\overline{\mathbf{D}}_x^x$ for the x-direction is given by

$$\overline{\mathbf{D}}_x^x = \frac{1}{\delta} \begin{pmatrix} 1 & -1 & 0 & \ldots & 0 & 0 \\ 0 & 1 & -1 & \ldots & 0 & 0 \\ \vdots & & & \ddots & & \vdots \\ 0 & 0 & 0 & \ldots & 1 & -1 \end{pmatrix} . \tag{60}$$

δ in Eq. (60) is the scaling parameter which determines the value above which a gradient is emphasized and below which it is smoothed. According to the principles of half-quadratic regularization,[5] the weighting coefficients $(b)_k$ in Eq. (58) are given by the expression $(b^{\nu+1})_k = \phi'(D\,f)/2(D\,f)$ where the potential function $\phi(t)$ was chosen to be $\phi(t) = t^2/(1+t^2)$. With $\phi'(t)/(2t) = 1/((1+t^2)^2)$ one can see that for $t \longrightarrow \infty$ $b = 0$ and for $t \longrightarrow 0$ $b = 1$. So the larger the gradient components, which are expressed by t, the less is the local regularization penalty. The strategy to compute the regularization weights can be summarized as follows: First, the regularization weights are computed from the last scatterer update with the proposed potential function $\phi(t)$. These regularization weights $(b^{\nu+1})_k$ are used and kept constant for the computation of the next scatterer update via DBIM. From this new scatterer update the next set of regularization weights is computed and the DBIM iteration process is repeated.

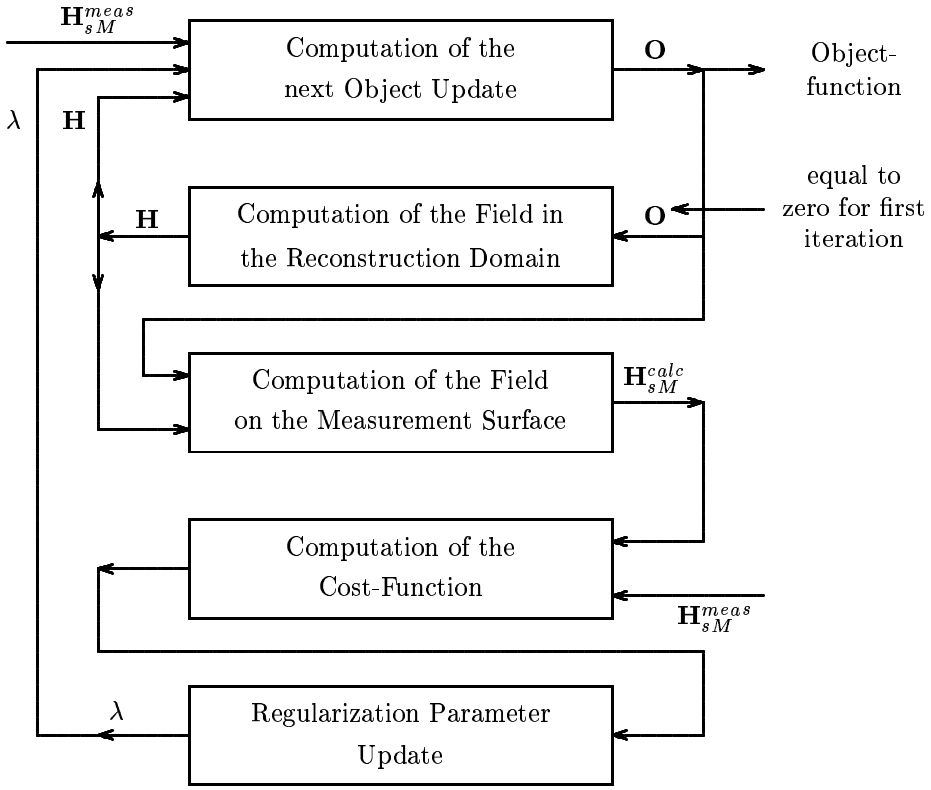

Figure 3. Iteration Process of the DBIM

In addition, as mentioned before, through the regularization smoothed domains are clipped off to reduce the computational burden further. After these domains are clipped, they are not considered in the subsequent iteration process any longer. λ in Eq. (57) is the global regularization parameter with which the condition number of the matrix in Eq. (57) can be adjusted.

4.1. ITERATION SCHEME

In the following we want to summarize all the steps necessary to compute the next scatterer update:

First, we start with the initial guess that the scatterer is equivalent to the background so that the total field is approximated by the incident field. After the first scatterer reconstruction, the total field in the reconstruction domain is computed as many times as the number of different incident field directions and frequencies. From this results and the previous scatterer reconstruction, the scattered field on the measurement surface can be computed. The error between the measured and the scattered field can be determined by

$$F^{\nu+1} = \frac{||\text{Measured field data} - \text{Computed field data}^{\nu}||}{||\text{Measured field data}||}\,. \tag{61}$$

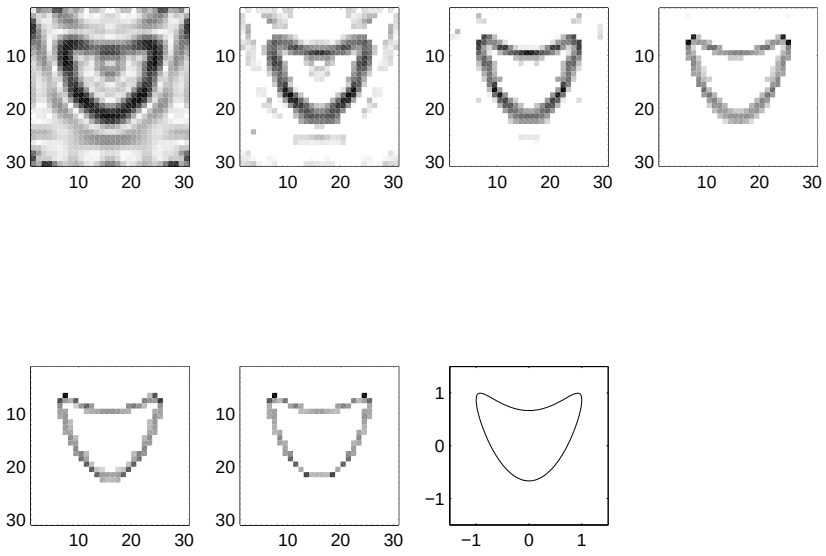

Figure 4. Reconstruction of a 'single kite' with single-frequency excitation $k = 5.1$, 16 incident sources around the reconstruction domain and 100 observation points on a circular measurement surface

The location dependent regularization weights $(b^{\nu+1})_k$ are computed as explained in Section 4. The next scatterer update can now be computed from the new regularization parameter weights, and the total field which was computed from the last scatterer update. The whole iteration process is depicted in Figure 3 once more. Here, ν is the current iteration stage in the DBIM process.

5. RECONSTRUCTION CONFIGURATION AND NUMERICAL RESULTS

A circular aperture S_M was used on which the synthetic scattered field data were compared in equidistant observation samples with the computed scattered field data of the last reconstructed scatterer update. A quadratic reconstruction domain was chosen. It was illuminated from all directions with the incident fields in equidistant angles around the reconstruction domain.

Figures 4 to 6 show the reconstruction results of a metallic two-dimensional scatterer using the DBIM and MLFMA for the forward as well as for the inverse solver. For all the numerical results, the reconstruction domain was chosen to be 3.0×3.0 meters. A single- or multi-frequency incident field excitation was chosen around the scatterer domain with a polarization orthogonal to the cylinder axis of the scatterer cross-section (TE-case). The metallic scatterer was enclosed by a circular measurement surface where the synthetically generated data were sampled in equispaced angles.

REFERENCES

1. W.C. Chew and Y.M. Wang, *Reconstruction of two-dimensional permittivity distribution using the distorded Born iterative method*, IEEE Trans. Med. Imaging **9**, pp. 218-225, 1990.
2. N. Joachimowicz, C. Pichot and J.P. Hugonin, *Inverse scattering: an iterative numerical method for electromagnetic imaging*, IEEE Trans. Ant. Prop. **39**, pp. 1742-1751, 1991.
3. C.-C. Lu and W.C. Chew, *A multilevel algorithm for solving a boundary integral equation of wave scattering*, Microwave Opt. Technol. Lett. **7**, pp. 466-470, 1994.
4. J.M. Song and W.C. Chew, *Multilevel Fast-Multipole Algorithm for solving combined field integral equations of electromagnetic scattering*, Microwave Opt. Technol. Lett. **10**, pp. 14-19, 1995.
5. P. Charbonnier, L. Blanc-Féraud, G. Aubert, and M. Barlaud, *Deterministic edge-preserving regularization in computed imaging*, IEEE Trans. Image Processing **6**, pp. 298-311, 1997.
6. P. Lobel, L. Blanc-Féraud, C. Pichot and M. Barlaud, *A new regularization scheme for inverse scattering*, Inverse Problems **13**, pp. 403-410, 1997.

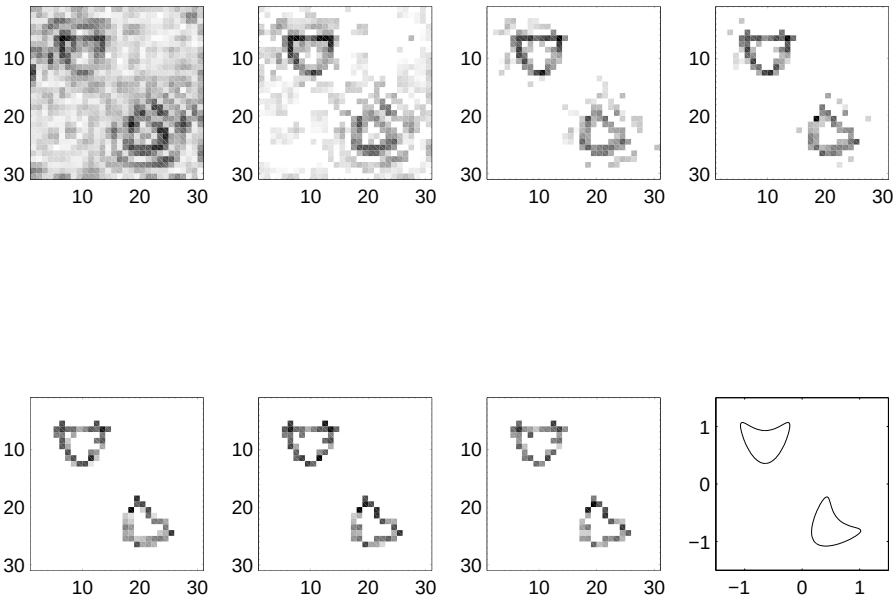

Figure 5. Reconstruction of a 'double kite' with single-frequency excitation $k = 7.6$, 16 incident sources around the reconstruction domain and 250 observation points on a circular measurement surface

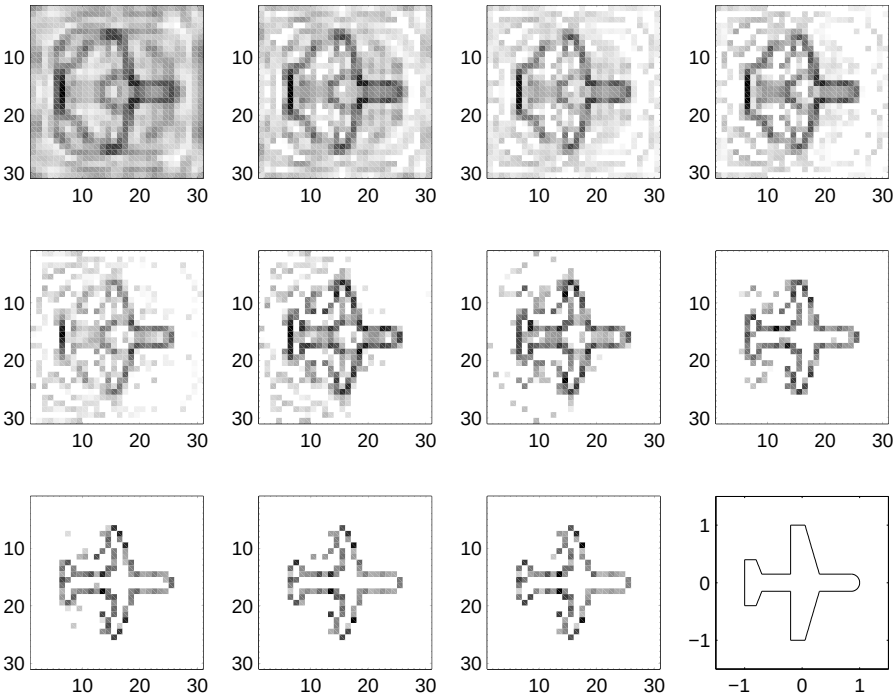

Figure 6. Reconstruction of an airplane model with multi-frequency excitation: 4 frequencies from $k_{min} = 1.5$ to $k_{max} = 9.2$ with 16 incident sources around the reconstruction domain and 250 observation points on a circular measurement surface